Journal of ELECTRONIC MATERIALS, Vol. 35, No. 5, 2006 *Regular Issue Paper*

Mechanical Properties of Intermetallic Compounds on Lead-Free Solder by Moiré Techniques

ITING TSAI,[1] ENBOA WU,[2] S.F. YEN,[3] and T.H. CHUANG[3]

1.—Institute of Applied Mechanics, National Taiwan University, Taiwan, R.O.C. 2.—Hong Kong Applied Science and Technology Research Institute Company Limited; email enboa@astri.org. 3.—Department of Materials Science and Engineering, National Taiwan University, Taiwan, R.O.C.

In this paper, methods for determining elastic moduli and coefficients of thermal expansion (CTE) of intermetallic compounds (IMC) formed at the interfaces between lead-free solder and metal substrates are presented. For the determination of elastic moduli, two kinds of lead-free solder—SnZn and Sn—were used; the metal substrates were copper and nickel. Nanoindentation techniques were adopted to determine the elastic moduli of $Cu_{33.5}Zn_{66.6}$, Cu_3Sn, Cu_6Sn_5, and Ni_3Sn_4. Results for $Cu_{33.5}Zn_{66.6}$ are new to the literature, and others values are in good agreement with those presented in the literature. On the other hand, for CTE determination, two moiré techniques, namely reflection moiré and shadow moiré, were developed to measure the deformation of IMC/metal composite structures subjected to thermal loading. Finite-element analyses using ANSYS were then performed as a convolutional process, and the genetic search algorithm was used to optimally obtain the CTE of IMC. The CTE of $Cu_{33.5}Zn_{66.6}$ was found to be approximate to that of copper, and the CTE of Cu_3Sn was 10% larger. This method is also applicable to on-wafer films and IMC on micrometer order, such as the case of solder/IMC/under bump metallization.

Key words: Intermetallic compound (IMC), lead-free, coefficients of thermal expansion (CTE)

INTRODUCTION

Intermetallic compounds (IMCs) are formed when interconnections in integrated circuit (IC) packages are jointed with solder. Although IMCs are not present in large amounts, they usually have a dominant influence on the reliability of the interconnections because of their characteristic material properties. The effect is even more severe when the IMC forms a continuous layer between the interface of solder and the thin metal layer of joints. Individual mechanical properties of a solder/IMC/under bump metallization (UBM) layered structure are required for simulation and analyses of the interconnection reliability, but they are always difficult to determine because the thickness of each layer is on the order of micrometers. Furthermore, it is often impossible to separate each thin layer for testing with commercially available testing machines. Therefore, little has been reported concerning both elastic moduli and coefficients of thermal expansion (CTE) of IMCs formed from soldering reactions to date.

Nanoindentation techniques have been applied to investigate the properties of microscale materials for years. Their extended capabilities are still under exploration, and applications to IMC material properties have emerged only recently.[1–4] In this paper, nanoindentation techniques were adopted to determine the elastic moduli of four different IMCs.

High-accuracy optical measurement techniques have been widely developed in various areas owing to their noncontact and whole-field properties. To quantify the interfering fringe patterns and to improve the resolution, phase-stepping, phase-unwrapping, and image-processing techniques were required and developed.[5–7] Asundi used the computer generated logical moiré in both static and dynamic applications.[6] Chiang measured the stress in thin films by rotating the grating 90° to form slope fringe patterns in the other orthogonal direction.[8] However, rotating or shifting the grating might not be suitable for real-time measurement under a variable temperature.

(Received October 7, 2005; accepted January 3, 2006)

We present herein a new method for obtaining the CTE of IMCs formed at the interface between lead-free solders and substrates. The elastic moduli of IMCs applied to ANSYS finite-element analyses as the inputs of the mechanical properties were determined first with nanoindentation techniques. The genetic search algorithm was then used to inversely obtain the CTE of the IMC, which made the deviation between the measured and ANSYS-calculated deformation minimal. To measure the deformation responses, reflection moiré and shadow moiré were adopted. We also developed an artificial cross grating for reflection moiré to overcome the problems of measurement under temperature change while preserving the improved resolution and the two orthogonal slopes at the same time.

METROLOGY TECHNIQUES

Techniques of high-accuracy optical measurement have mushroomed in precision metrology owing to their noncontact and whole-field properties. Two moiré methods, shadow moiré and reflection moiré, were adopted in this study. Shadow moiré is a well-established optical technique used for the measurement of the out-of-plane displacement, and reflection moiré is used for the partial derivative (slope) of the out-of-plane displacement, in the principal direction of the grating. Numerical differentiation is known as an inaccurate process, and as such it should be avoided if possible. In this regard, reflection moiré, with its slope as the prime experimental data, is superior to displacement-generating methods such as shadow moiré and holography. The essentiality of the reflecting sample surface was regarded as the major limitation to its application. Nevertheless, it is favorable for our applications to metallic shinning IMCs and mirror-like surfaces, such as silicon substrates.

The key points in this part are focused on the implementation of the redeveloped reflection moiré. A schematic diagram of the experimental setup is shown in Fig. 1. The sample used to demonstrate the measurement procedure is a 2.5 cm × 2.5 cm × 350 μm (100) silicon substrate with a 2-μm copper film deposited on the bottom surface. A parallel white light passed through the grating and the beam splitter and was then reflected from the surface of the sample. The deformed grating was the reflection of the cross grating and was recorded by the charged couple device (CCD), which is shown in Fig. 2a. A cross grating was employed to measure the slope change of the two orthogonal directions. To separate out the information of the first direction, the grating of the second direction had to be removed. A 1-by-5 convolution kernel was used as an averaging filter,[9] and the dimensions of the kernel were determined by the number of pixels of one recorded grating pitch. The intensity of the filtered frame can be written as

$$I_i(x,y) = a(x,y) + b(x,y)\cos[2\pi f_0 x + \phi_i(x,y)] \quad (1)$$

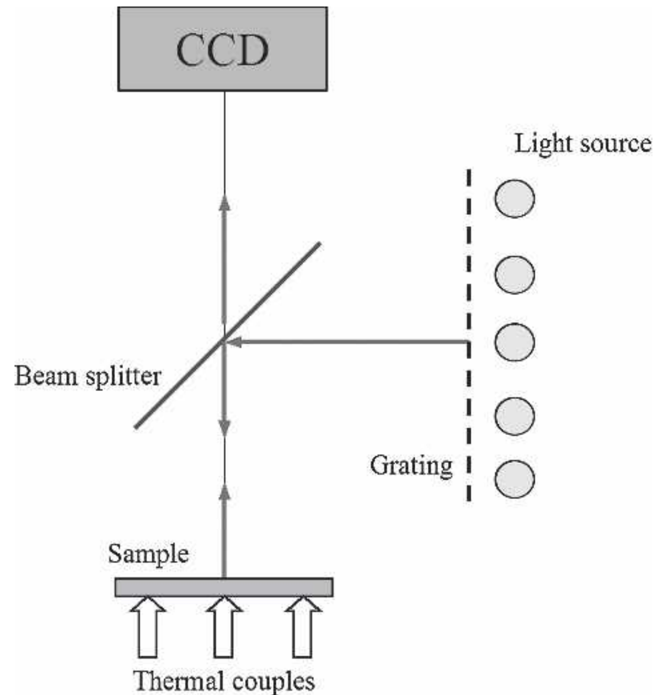

Fig. 1. Schematic diagram of the experimental setup of reflection moiré.

where the phase $\phi_i(x,y)$ contains the desired information, $a(x,y)$ is the background intensity, $b(x,y)$ is the fringe modulation intensity, and f_0 is the spatial-carrier frequency. To extract the phase from the intensity distribution, phase shifting was needed, and this was accomplished by numerically shifting a computer generated grating instead of using an optically shifting mechanism. Any step length can be achieved with numerical shifting, and we chose the Carré four-step formula with a $\pi/2$ shift, which is more stable and can cancel out nonlinear terms automatically.[10] The extracted term $[2\pi f_0 x + \phi_i(x,y)]$ can be shown as the wrapped-phase map, as in Fig. 2b, and the profile of the dashed line is shown in Fig. 2c. After the wrapped phase is unwrapped, a continuous distribution of the phase can be obtained (Fig. 2d). If the sample undergoes a temperature change, we can record the deformed grating at any temperature. With the same procedure, another unwrapped phase $[2\pi f_0 x + \phi_f(x,y)]$ can also be obtained. The phase of slope under any temperature change, $\Delta\phi = (\phi_f - \phi_i)$, can be obtained by subtracting these two phase maps. The phase related to the experimental setup is as follows:

$$\Delta\theta = \frac{Np}{2L}, N = \frac{\Delta\phi}{2\pi} \quad (2)$$

where $\Delta\theta$ is the slope change, N is the order of the interfering fringe, p is the grating pitch, and L is the distance from the grating to the sample surface. With p = 400 μm and L = 0.69 m in our case, the resolution is 2.9×10^{-4} rad/fringe. Furthermore, the resolution can be enhanced to the order of 10^{-6} rad/pixel with the phase-shifting techniques

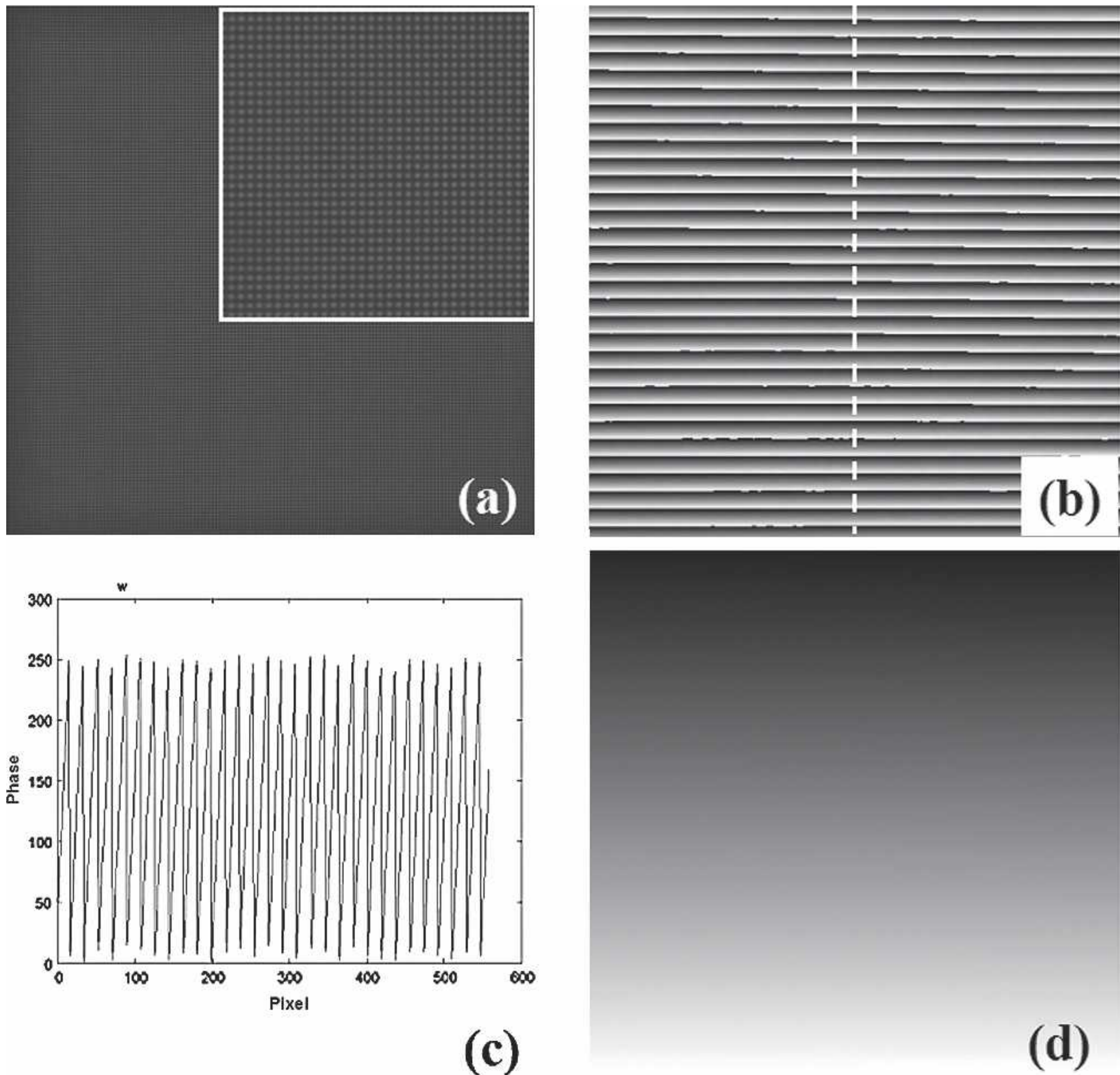

Fig. 2. (a) Deformed grating recorded by the CCD. (b) Warped phase map. (c) Profile of the dashed line in (b). (d) Continuous distribution of the phase:unwrapped phase map.

mentioned above, which can be equivalently converted to a resolution of 0.2 μm for warpage in a 2.5-cm square area.

In addition to the extremely high resolution with relatively coarse grating pitch needed, reflection moiré possesses the capability of visualizing the sample condition, which is usually not accessible with laser scanning measurement. An example of a bilayer structure, a 2 μm copper film deposited on a silicon substrate, is illustrated in Fig. 3. Partial delamination of the copper film caused a small bulge on the copper surface. The topography of the copper-film surface with the small bulge on it could be measured with shadow moiré (Fig. 3a). When we turned the specimen over and measured the reverse silicon surface with reflection moiré, this high-resolution and whole-field measurement allowed the delamination to reveal even the bulge on the other side (Fig. 3b).

The techniques developed for reflection moiré to quantify fringe patterns and to improve the resolution, including phase stepping, phase unwrapping, and image processing, can also be applied to shadow moiré, as has been described in detail elsewhere.[7] It is notable for shadow moiré that, for general application, it uses a grating pitch finer than 100 μm to attain a resolution of 10 μm. However, reflection moiré can bear a relatively coarse grating pitch,

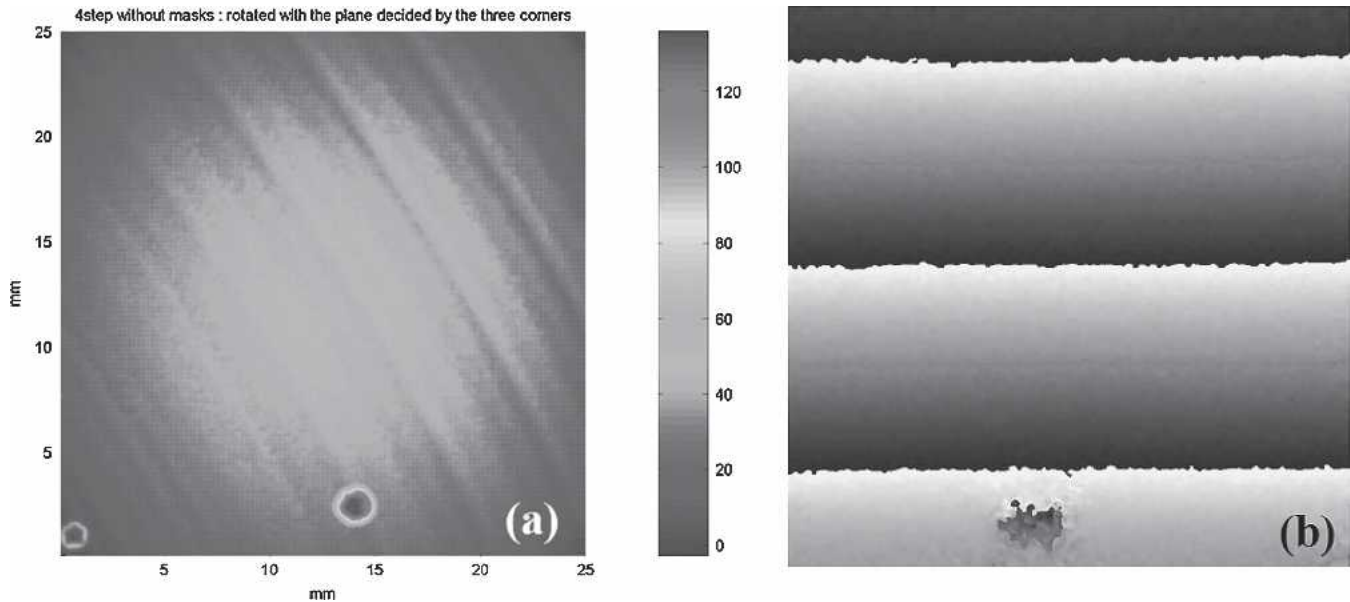

Fig. 3. (a) Topography measured from the copper-film surface with shadow moiré. (b) Warped phase map of the copper-film/silicon sample with reflection moiré.

such as 400 μm, to equivalently obtain the resolution of 0.2 μm for warpage, which also efficiently lowers the cost of grating fabrication.

MECHANICAL PROPERTIES OF INTERMETALLIC COMPOUNDS

For IMC materials, two types of lead-free solder were used, namely SnZn and Sn. The metal substrates used were copper and nickel. With a nanoindentor (UMIS II, CSIRO, Australia), the elastic moduli of different IMCs were determined. The IMCs we used in this paper included $Cu_{33.5}Zn_{66.5}$, Ni_3Sn_4, Cu_6Sn_5, and Cu_3Sn. The nanoindentor was equipped with a Berkovich diamond-probe tip with a 200-nm tip radius. As for analysis methods, the multiple-point unloading method by Oliver and Pharr was used to determine the elastic modulus of each indent, with Poisson's ratio set at 0.3.[2]

Cu-Zn Intermetallic Compounds

SnZn solder is considered to be a promising lead-free solder because of its lower melting point. However, there is almost no information on the material properties of Cu-Zn IMC so far. For the IMC mechanical property determination using SnZn solder, specimens were prepared by dipping the copper substrate, which was 2.0 cm × 2.0 cm × 0.060 cm, into a SnZn bath to overcome the poor wetting problem. The SnZn bath was made by combining 91 wt.% Sn and 9 wt.% Zn in a crucible melt at 400°C on a hotplate until well mixed. Caution and post-processing were needed to ensure that the solder attached to only one surface. After the soldering reaction and annealing at 250°C for 30 min., a uniform layer of $Cu_{33.5}Zn_{66.5}$ IMC with a thickness of up to 20 μm was then formed (Fig. 4). The SnZn solder was removed by mechanical grinding, and the surface of the IMC was polished first with 1.0-μm and then with 0.3 μm alumina suspensions. Surface roughness is a key factor that affects the test data. A rough surface often causes great variations in the results. Therefore, the particle size of the final polishing is also critical. The specimen was pressed ten times with the nanoindentor for each different maximum depth. The average value for the elastic modulus was recorded to be 158 GPa, with minimum variation in values.

To measure the coefficient of thermal expansion, the Cu-Zn IMC/copper specimen was heated on the hotplate at 150°C for 10 min. and then taken off of the hotplate and placed carefully on a tripod made up of three thermal couples. The experimental setup is illustrated in Fig. 2. The frame of the initial state was taken at 65°C, and the final frame was taken at 25°C. With the abovementioned numerical

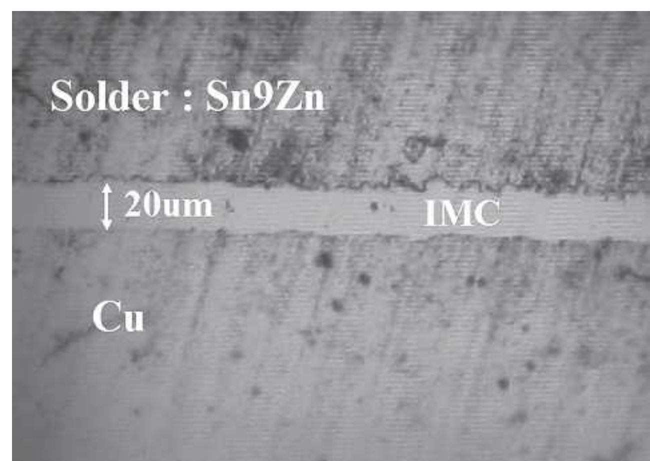

Fig. 4. Cross-section image of Cu-Zn IMC with the optical microscope.

phase-shifting techniques, the slope of the sample due to the temperature change of 40°C was then obtained. However, there was no evident slope, even with a high resolution on the order of 10^{-6} rad/pixel. With the dimensions of the sample mentioned above, the difference between the CTE of copper and that of $Cu_{33.5}Zn_{66.5}$ can be estimated as less than 1 ppm/°C, which is less then 5% of the CTE of the copper. Therefore, the CTE of $Cu_{33.5}Zn_{66.6}$ can be determined to be approximate to that of copper.

Cu-Sn Intermetallic Compounds

In order to grow a uniform Cu-Sn IMC layer, electroplating was used to make an even tin layer on copper substrates with dimensions of 1.5 cm × 1.5 cm × 0.050 cm. After the soldering reaction and annealing, there existed two phases of Cu-Sn IMC: Cu_6Sn_5 and Cu_3Sn. For the sample of Cu_6Sn_5, about 38 μm of tin was electroplated on the copper substrate for 25 min. For the Cu_3Sn sample, in order to grow a layer of Cu_3Sn without Cu_6Sn_5, a thinner tin layer of 20 μm was electroplated. The thinner tin layer shortened the time needed to make all of the Cu_6Sn_5 transfer to Cu_3Sn. After a solid-state soldering reaction at 220°C for 80 hr and annealing at 325°C for 60 hr, the Cu_6Sn_5 sample had a layer of IMC with 16-μm Cu_6Sn_5 and 10-μm Cu_3Sn, which is shown on the left in Fig. 5. In the Cu_3Sn sample, almost all of the Cu_6Sn_5 was transferred to Cu_3Sn, as is shown on the right of Fig. 5. The procedure to remove the solder was the same as that for the Cu-Zn samples. The only difference was that the final polishing particle size was reduced to 0.05 μm. With the nanoindentor, average values of the elastic moduli were determined to be 124 GPa for Cu_6Sn_5 and 143 GPa for Cu_3Sn.

The warpage change of the two-layer structure with 9.8-μm Cu_3Sn and 52.6-μm copper foil under temperature change was adopted for the CTE of the Cu_3Sn. The dimensions of the sample were 3.0 cm × 2.0 cm. In the tensile experiment, a strip of 5.5 cm × 1.0 cm × 80 μm copper foil with one end fixed was used. The tensile loading was applied to the other end by a force gauge. With a strain gauge in the middle of the specimen, the elastic modulus of copper foil was determined to be 100 GPa. Instead of reflection moiré, which has better resolution, shadow moiré was applied because the initial deformation of such a thin foil is too large for the depth of field (DOF) of reflection moiré, and the sample was too flexible to form a good-quality reflective surface. With proper design of the dimensions of the specimen, the resolution of shadow moiré is sensitive enough to serve the purpose. The warpage of the sample was measured at room temperature, 60°C, 100°C, 140°C, 180°C, and 220°C in the oven with shadow moiré. The first measurement did not show monotonic change of warpage with increasing temperature. After cooling for 24 hr, the measurement was carried out again, and the relation between warpage and temperature became linear (as shown in Fig. 6), because the initial state of the sample had accumulative residual deformation, such as reflow from the temperature for IMC annealing and sample trimming. In the first thermal loading, release of the residual stress did not allow the warpage to follow the increasing temperature. Finite-element analyses using ANSYS were applied to the Cu_3Sn/copper foil composite structure under changing temperature. The genetic search algorithm was used to optimally obtain the CTE of the Cu_3Sn, which made the deviation between the measured and ANSYS-calculated warpages minimal. The CTE of the Cu_3Sn

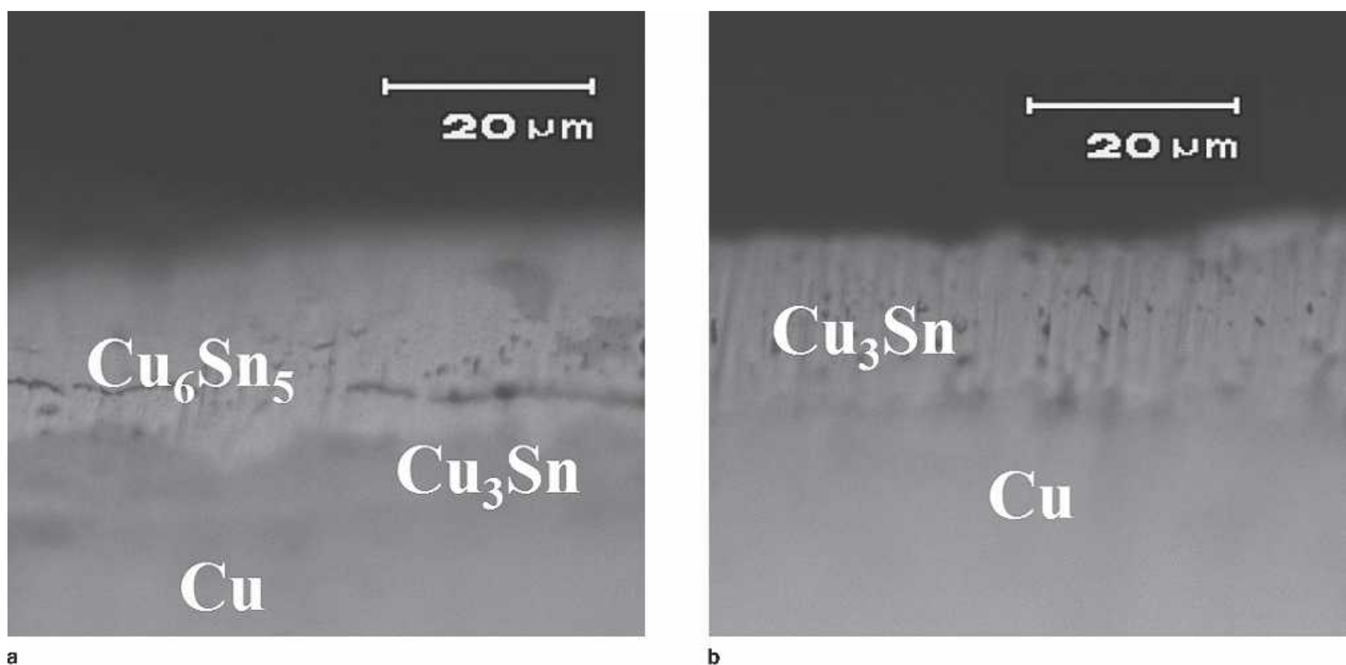

Fig. 5. Cross section of samples with Cu-Sn IMCs.

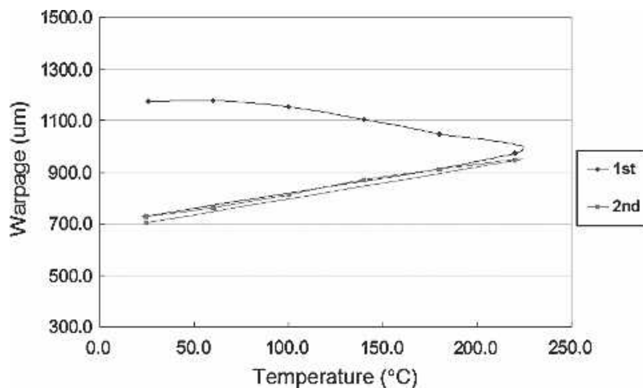

Fig. 6. Warpage vs. temperature of Cu_3Sn/copper foil structure.

was determined to be 18.2 ppm/°C, which is approximately 10% greater than that of copper. Figure 7 shows that the experimental results were in good agreement with the finite-element model. We focused on the material properties of Cu_3Sn instead of those of Cu_6Sn_5 because its interface with the thin metal layer is usually where the failure happens.

Ni-Sn Intermetallic Compounds

As for the Ni_3Sn_4 IMC, tin layers 40 μm thick were electroplated onto the nickel substrate. After a soldering reaction at 220°C for 80 hr and annealing at 325°C for 93 hr, the tin was exhausted, and a layer of Ni_3Sn_4 about 45 μm thick had formed. The morphology of Ni_3Sn_4 shows it has a much more even interface than Cu-Sn IMCs, as can be seen in Fig. 8. The post-processing was exactly the same as that for the Cu-Sn IMC, and the elastic modulus was determined to be 152 GPa. This 1-mm-thick nickel substrate was also tested with the nanoindentor to determine the elastic modulus, which was determined to be 213 GPa and consistent with the general value.

DISCUSSION

The list of the elastic moduli of IMCs, together with the results in the literature, is shown in Table I.

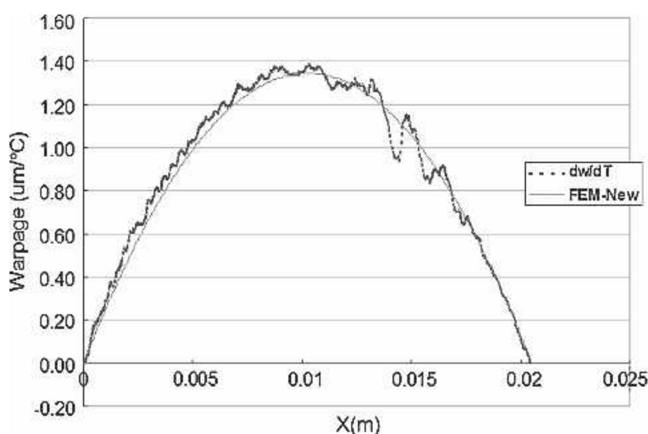

Fig. 7. Warpage change from the experiment and finite-element analysis under unit temperature change (°C).

Fig. 8. Cross section of Ni_3Sn_4.

It is difficult to compare the results from nanoindentation with Fields' results because the samples used by Fields were produced with a hot isostatic press instead of an actual solder joint, and the experimental technique was also different.[11] This study presents the same elastic modulus of Cu_3Sn as that in most of the literature in which nanoindentation was applied, and the elastic modulus of Cu_6Sn_5 falls in the average of all the values reported in the literature. On the basis of the consistent results for Cu_3Sn and Cu_6Sn_5, the data on $Cu_{33.5}Zn_{66.5}$ and Ni_3Sn_4 can be considered reliable in this study.

Table II lists the CTEs of IMCs in the literature, and the sample preparation is also described. The records of the CTEs of IMCs are limited, and we have not found reports in which IMCs were adopted directly from soldering reactions so far, except for this study. The CTE of this study is in good agreement with that of bulks measured with other methods.[11,12] The proportional intensity of x-ray diffraction (XRD) for Cu_3Sn is shown in Fig. 9. The Cu_3Sn from copper foil in this study is consistent with the distribution of that from bulk in the database, which also reveals the reason that the CTE and elastic modulus of Cu_3Sn in this study match the records in the literature well. The correspondence between the out-of-plane elastic modulus of Cu_3Sn obtained with nanoindentation in this study and the in-plane ones in the literature is also consistent with the bulk properties illustrated with the XRD data. According to the results presented above, the methodology developed in this study for CTE measurement of IMCs is competent and successful.

From the results of this study for Cu_3Sn vs. copper, there is no severe difference in elastic moduli and CTE between the IMC and the metal substrate. It is probably other material properties that have a dominant effect on the failure of the interface between the IMC and the substrate. Hardness and toughness are potential candidates. From the results of Chromik, the hardness of copper is 1.7 GPa, and that of Cu_3Sn is 6.2 GPa.[1] Hardness inhomogeneity might cause stress concentration at or near the interface between the IMC and the metal substrate or solder. In addition, brittle IMCs with low toughness near the interface where stress concentrates have a tendency to initiate or propagate cracks.

Table I. List of Elastic Moduli of IMCs

Researchers	Experimental Techniques	Elastic Modulus (GPa)			
		$Cu_{33.5}Zn_{66.5}$	Cu_6Sn_5	$Cu_{3+}Sn$	Ni_3Sn_4
This study	Nanoindentation	158	124	143	152
Chromik et al.[1]	Nanoindentation	—	119	143	—
Lee et al.[3]	Nanoindentation	—	132	143	—
Duh et al.[4]	Nanoindentation	—	125	136	143
Fields et al.[11]	Compression	—	86	108	133

Table II. List of CTE of IMCs

Researchers	IMC	Sample Description	Measurement Techniques	CTE (ppm/°C)
This study	Cu_3S_n	Electroplated Sn/Cu foil Soldering reaction	Shadow morié, GA	18.2
Fields et al.[11]	Cu_3Sn	Bulk specimens Rapid solidification Hot isotatic press	ASTM E 228	19.0
Cotts et al.[12]	Cu_3Sn	Bulk specimens Rapid solidification Are melting, annealing	TMA	18.2
This study	$Cu_{33.5}Zn_{66.5}$	Dipping Sn-9Zn bath/Cu metal Soldering reaction	Reflection morié, GA	17.5

CONCLUSION

We have presented a new method for obtaining the CTEs of IMCs formed at the interface between lead-free solders and substrates. To successfully determine the CTE using the method developed in this study, the first challenge is to produce a flat and uniform layer of IMC on the substrate, and the area needs to be large enough to suit the resolution of the metrology methods adopted. Dipping for Sn-9Zn and electroplating for Sn were used to fulfill this purpose. To measure the deformation responses, we also developed an artificial cross grating for reflection moiré to overcome the problems of measurement under temperature change while preserving the improved resolution and the two orthogonal slopes. A nanoindentor was applied to determine the elastic moduli of $Cu_{33.5}Zn_{66.5}$, Cu_6Sn_5, Cu_3Sn, and Ni_3Sn_4, with the assumption that Poisson's ratio was 0.3 for all samples. The results with Cu_6Sn_5 and Cu_3Sn agreed well with those of previous publications in which nanoindentation was applied. The results with Ni_3Sn_4 are limited, and those with $Cu_{33.5}Zn_{66.5}$ from Sn-9Zn are new. The CTE of $Cu_{33.5}Zn_{66.6}$ was found to approximate that of copper. The deviation was within the resolution of the phase-shifting reflection moiré using the method developed in this study. On the other hand, with the phase-shifting shadow moiré and the search algorithms developed in this study, we also obtained the CTE of Cu_3Sn, which was approximately 10% larger than that of copper and also consistent with that of the bulk specimens in the literature. The XRD result also matched that of the bulk specimens in the database.

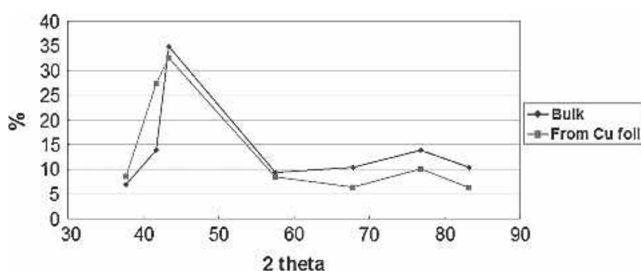

Fig. 9. Proportional intensity of XRD for Cu_3Sn.

ACKNOWLEDGEMENT

The authors sincerely acknowledge the financial support from the National Science Council, Taiwan, for this research (Grant NSC-94-2216-E002-015). The authors thank the Nano Center for Science and Technology, National Taiwan University, for permission to use the nanoindentor. The work was also partially supported by VIA Technology, Inc., ROC, and the Electrical Research Service Organization (ERSO) of the Industrial Technology Research Institute (ITRI), Taiwan, ROC.

REFERENCES

1. R.R. Chromik, R.P. Vinci, S.L. Allen, and M.R. Notis, *J. Mater. Res.* 18, 2251 (2003).
2. J.S. Kang, R.A. Gagliano, G. Ghosh, and M.E. Fine, *J. Electron. Mater.* 31, 1238 (2002).

3. M. Lee, Y. Hwang, M. Percht, J. Park, Y. Kim, and W. Liu, 2004 Electronic Components and Technology Conf. Proc. (Piscataway, NJ: IEEE, 2004), pp. 901–905.
4. G.Y. Jang, J.W. Lee, and J.G. Duh, *J. Electron. Mater.* 33, 1103 (2004).
5. C.A. Sciammarella, *Exp. Mech.* 22, 418 (1982).
6. A. Asundi, *Exp. Mech.* 34, 230 (1994).
7. I. Tsai, C.Z. Tsai, E. Wu, and C.A. Shao, *Proceedings of IMAPS Taiwan Technique Symposium* (Washington, D.C.: IMAPS, 2001), pp. 290–297.
8. F.P. Chiang, *Exp. Mech.* , 377 (1972).
9. *Image Processing Toolbox User's Guide* (Natick, MA: The MathWorks, Inc., 1997).
10. K. Creath, *Prog. Opt.* 26, 351 (1998).
11. R.J. Fields, S.R. Low III, and G.K. Lucey, Jr., *The Metal Science of Joining*, ed. M.J. Cieslak, J.H. Perepezko, S. Kang, and M.E. Glicksman (Warrendale, PA: TMS, 1992), pp. 165–173.
12. N. Jiang, J.A. Chromik, and E.J. Cotts, *Scr. Mater.* 37, 1851 (1997).